Int J Adv Manuf Technol (2018) 94:13–29
DOI 10.1007/s00170-016-9481-8

ORIGINAL ARTICLE

A robust butt welding seam finding technique for intelligent robotic welding system using active laser vision

Jawad Muhammad[1] · **Halis Altun**[2] · **Essam Abo-Serie**[3]

Received: 5 March 2016 / Accepted: 15 September 2016 / Published online: 14 October 2016

Abstract Intelligent robotic welding requires automatic finding of the seam geometrical features in order for an efficient intelligent control. Performance of the system, therefore, heavily depends on the success of the seam finding stage. Among various seam finding techniques, active laser vision is the most effective approach. It typically requires high-quality lasers, camera and optical filters. The success of the algorithm is highly sensitive to the image processing and feature extraction algorithms. In this work, sequential image processing and feature extraction algorithms are proposed to effectively extract the seam geometrical properties from a low-quality laser image captured without the conventional narrow band filter. A novel method of laser segmentation and detection is proposed. The segmentation method involves averaging, colour processing and blob analysis. The detection method is based on a novel median filtering technique that involves enhancing of the image object based on its underlying structure and orientation in the image. The method when applied enhances the vertically oriented laser stripe in the image which improves the laser peak detection. The image processing steps are performed to make sure that the laser profile is accurately extracted within the region of interest (ROI). Feature extraction algorithm based on pixels' intensity distribution and neighbourhood search is also proposed that can effectively extract the seam feature points. The proposed algorithms have been implemented and evaluated on various background complexities, seam sizes, material type and laser types before and during the welding operation.

Keywords Seam finding · Robotic welding · Computer vision · Feature extraction · Intelligent sensors · Robotic application

✉ Jawad Muhammad
mohdjawadi@yahoo.com

Halis Altun
halisaltun@gmail.com

Essam Abo-Serie
essamaboserie@gmail.com

[1] Graduate School of Natural and Applied Sciences, Alaeddin Keykubat Yerleskesi, Selcuk Universitesi, 42250 Konya, Turkey

[2] Department of Electrical and Electronics Engineering, Karatay University, Konya, Turkey

[3] School of Mechanical, Aerospace and Automotive Engineering, Coventry University, Coventry, UK

1 Introduction

Research in vision-based intelligent robotic welding is one of the most rapidly growing areas for robotic applications. However, to a large extent, teaching strategy of the robot for the welding task remains '*teach and playback*'. Hence, fully automated robotic welding system is yet to be effectively achieved. This is due to harsh environmental conditions of welding and various factors such as welding spatter and arc light disturbance, welding material types, distortions due to welding heat generation and varying structure of the welding seams [1]. Intelligent robotic welding system comprises of three basic components: (1) tracking and profiling of welding seam and pool, (2) robot trajectory planning and control and (3) parameter control of welding process []. Robot trajectory planning and control involves teaching of the robot to follow the welding seam path, at a specific welding torch orientation, and perform the required welding task efficiently. Intelligent methods for the path planning have been proposed by researchers [–4]. The path to follow and the orientation of the torch to be set depend on the welding process parameters and

the welding seam geometrical properties. To achieve high-quality welding, the process parameters need to be effectively controlled. Researchers have proposed various techniques to control the process parameters [5–8]. However, these techniques depend on the geometrical measurements of the welding bead and seam before, during and after the welding process. The geometrical measurements are obtained through the tracking and profiling of welding seam and pool. Methods in tracking and profiling welding pool and seam can be categorised into (i) optical sensing and (ii) non-optical sensing methods. One of the most popular non-optical sensing method is the *through-arc sensing* method [1, 8, 9]. Optical sensing method can be further categorised based on either *passive vision* or *active vision* methods. The distinction between these two methods relies on the use of the optional light source. In the *active vision*, a camera device and a light source are used, while in the *passive* vision, two camera devices are used without a light source. In passive vision, due to the complex nature of the welding environments, wide range of methods had been proposed by researchers [10–17]. Using the passive vision system, two set of information can be obtained: (1) the seam profile which can alternatively be acquired by using active vision and (2) the welding pool profile which can only be acquired with passive vision. More so, passive vision systems can be used to acquire the seam path holistically as oppose to active vision which only provide one point at a time. Numerous techniques have been proposed for the image preprocessing, seam profiling and weld pool profiling of the passive vision system. For the welding seam profiling, various methods are proposed such as grey-level distribution methods [10] that consider the darkness characteristic of the welding seam region, conventional edge detection methods like Canny edge detection [17], Sobel edge detection [11] that extract edges in the image from which the seam is then extracted and template matching methods [16] that searches for a known pattern in an image by using a predefined template which identifies the seam. For the welding pool profiling, the basic task is detecting the edges of the welding pool from which the pool dimensional features can be determined. Various methods have been proposed by researchers to detect the pool edges. Among which is the use of conventional edge detection methods [12] such as Canny and Sobel edge detection. Another notable technique is the histogram analysis methods [13] that analyse the histogram of the welding pool image in order to obtain the boundaries of the pool as the edges. In [14, 15], an analysis model and experimental technique on computing seam finding accuracy by using passive vision has been proposed; the serial work makes the path planning a further step forward in the passive vision field.

On the other hand, in the active vision system, the concept of triangulation is applied to find the seam geometrical properties. It employs a camera and a light source device to capture the image of the welding seam. A comprehensive survey of the active vision methods of seam finding has been performed [18]. Seam finding in the active vision can be simply broken down into two tasks: detecting the laser stripe in the image and extracting the feature points from the detected laser line that identify the seam.

The maximum intensity is the most common feature which is used for laser stripe extraction. Due to the high intensity values (higher brightness) at the region of the laser stripe, many authors proposed a simple technique which explores this characteristic of assuming maximum intensity to be the laser stripe position while extracting the laser stripe region from an image [19–24]. The idea behind the maximum intensity strategy is to consider every row or column separately as a 1D signal depending on the orientation of the laser stripe as either horizontal or vertical. For horizontal laser stripe, columns in the image are treated independently. The row position in each column that has the maximum intensity value is selected as a point in the laser stripe. Combining these points from all the columns together makes up the position of the laser stripe profile in the image. Sometimes, instead of taking one point with peak intensity, multiple peaks are chosen to produce a stripe of more than one pixel width, and the peaks are subsequently discarded based on definite criteria [19, 20, 23]. In [20, 23], the middle pixel among the multiple peaks is selected as the laser stripe profile location. In [21], after searching and combining pixel points with maximum intensity, those points caused by false imaging are rejected by using temporal and spatial continuity constraints and the profile is obtained by using linear interpolation and Gaussian filtering. In [22], five horizontal laser stripe lines are extracted by the maximum intensity method. The lines are extracted by sorting the intensity values sequentially in a decreasing order along each column and then taking the first five values as the position of the peaks for the five lines in that column. Instead of the traditional maximum intensity, a more accurate method is to obtain the peak position at sub-pixel accuracy [25–28]. The methods consider the imperfection of the laser stripe distribution which could make a pixel position of the peak erroneous. To accurately detect the peak at sub-pixel level, methods such as *Gaussian approximation* [25], *centre of mass* [25], *linear interpolation* [25], *Blais and Rioux* [24] detectors and *parabolic estimator* [25] are used. The distinction between these methods depends on the assumption of the intensity distribution of the laser stripe. Gaussian approximation and centre of mass assumed that the spread of intensity values across the stripe conforms to a Gaussian distribution. Linear interpolation assumes that a simple, linear relationship defines the spread of intensity values across the stripe. A comparative analysis on the effectiveness and accuracy of these sub-pixel methods was performed in [25]. The authors concluded that these methods display comparable performance within the same range.

After the laser stripe profile extraction, the turning point and corner points are then extracted as *feature points*. In an ideal condition, extracting these points could be a simple task of performing turning points or corner point detection. However, in reality, the extracted laser stripe is far from its ideal shape. The extracted stripe may experience discontinuities along the lines, and the noise could suppress the feature points into higher or lower than their actual values. This makes it more challenging to accurately detect these points. Researchers have proposed methods to efficiently detect these feature points. The use of split and merge algorithm [22, 29], second central difference (second CD) [20, 30], local maxima and minima [21, 24, 31–33] and rule-based techniques [27, 28, 34–37] have proven to be effective in extracting the *feature points*. In [22], the researchers make use of the combination of split and merge [38] and template matching method to determine the feature points. In the split and merge method, approximate straight line is generated from three points according to the turning angle between the points. The points in the stripe profile are scanned by considering three points at a time. A point is discarded as noise if the turning angle between the two lines, which are joining the three points, exceeds a certain threshold. The feature points are then extracted by comparing the generated straight line with a welding joint template. In [29], similar strategy of selecting the feature points based on computed turning angle of a point is proposed. The feature points are determined by set of rules based on the position and value of the turning angle at each point. For each of the feature points, there exist associated rules that define the nature of the point. In [20], a method based on the second CD of the row index of each point in a horizontally oriented laser stripe profile is proposed. First, the second CD is computed for all the points in the laser stripe. Based on the values of the second CD, a point scanning algorithm is proposed that searches for the feature points that meet predefined criteria. In [30], unlike in [20], a group of points that have CD value greater than the 70 % of the maximum CD value is selected and the centre point in the group is taken as the position of the feature points. The feature points can also be extracted as the local maxima and minima of the second derivative of the laser stripe profile [21, 24, 31–33]. The method involves computing the second derivative of the laser stripe, searching for the local minima and maxima and selecting the points that correspond to the local maxima and minima as the feature points. Another notable technique for extracting the feature points is the rule-based approach method [27, 28, 34–37]. The method involves approximation of the extracted laser profile into line segments. The line segments are labelled according to predefined welding segments. The labelled line segments are systematically combined to form a feature string. Based on certain defined criteria and classification methods, the feature string is interpreted to be one of the predefined welding joint type and the feature points are extracted from the joint.

In the aforementioned methods, single-channel images (grey images) are used because of the conventional narrow band filter usually installed on the camera to increase its sensitivity to the laser. The narrow band filter when used during welding may reduce the laser contrast with respect to the welding arc noise. This is because the most dominant noise in welding environment is the white light which is produced by the welding arc. As the white light contains all wavelength of light, the filter could not suppress the noise in the laser spectral band due to white light. This makes the camera to capture the laser and the white noise with similar intensity thereby reducing the laser contrast with respect to the welding arc noise. Also, the extracted position profile of the laser stripe could be noisy which affects adversely the performance of the feature point detection. Only few researches propose an additional processing to filter out the peaks. Furthermore, majority of the feature point extraction methods consider the feature points as corners and employ corner detection methods as the feature extraction. However, in the presence of a noise or low-quality laser, false corners are inevitable, and this can lead to catastrophic result. In this work, based on these issues, we proposed four major contributions: (1) sequential image processing steps that use the images of a low-quality cheap laser and accurately determine the position of the seam in it, (2) a proposed active vision system design without using a narrow band filter but with an additional software-based colour processing to increase the laser contrast with respect to the welding arc noise, (3) a novel laser profile pre-processing that involves enhancing the laser image with a novel oriented median filter. This filter enhances an object based on its underlying structure and orientation in the image. The method enhances the vertically oriented laser stripe in the image which improves the laser profile extraction; and (4) a proposed feature extraction algorithms that involves pixel neighbourhood search based on a detected laser base line. The points are extracted independently and irrespective of their turning angle or strategic position.

In the next section, the details of the system design and the proposed algorithms will be discussed followed by the result and discussions.

2 The proposed algorithm

2.1 System configuration

The proposed system comprises of a laser light source, a camera device and a welding robot. For the light source, a 5-mW laser with a wavelength of 650 nm was used. This wavelength was chosen according to the spectrum analysis of the welding process as shown in Fig. 1a. From the figure, it is evident that the arc light which has components in all over the spectrum is at its weakest intensity in the wavelength range of 620–

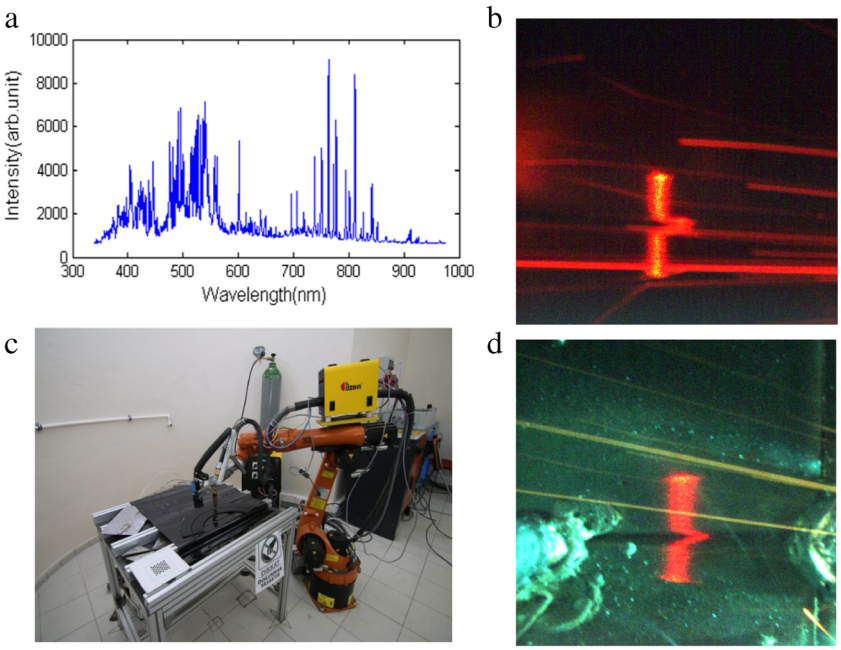

Fig. 1 **a** The spectral analysis of GMAW for low-carbon steel of Q235 [10]. **b** System configuration showing the camera, robot and welding machine. **c** Welding image with a narrow band filter and **d** welding without the narrow band filter

720 nm [10]. A DFK 23G274I Sony CCD GigE industrial camera device with a resolution of 1600 × 1200 was used. KUKA industrial welding robot coupled with CR-4 controller was used. Figure 1b shows the system configuration.

2.2 Proposed algorithm

The proposed algorithm comprises of two steps: (1) detection of the laser base line that represents the laser stripe without deformation and (2) seam feature point extraction. The aim of these algorithms is to extract the seam features that can be used for automatic teaching of the welding robot before the welding and for online tracking and control of the welding robot during welding process. In the following sections, the details of these steps will be described.

2.2.1 Laser base line detection

The proposed processing stages for detecting the base line consists of three steps: a pre-processing step, a laser peak point detection step and a line fitting step correspondingly.

Step 1: *Pre-processing*

The pre-processing stage is performed in order to remove unwanted objects in the image. Because the colour of the laser light in the image is predominantly red, a pre-processing technique is proposed that utilises this property. Usually, a narrow band optical filter is used with the camera to provide more sensitivity and selective selection of the red light with specific wavelength to pass through the camera. However, use of these filters is not flexible and during welding, it may reduce the laser contrast with respect to the welding white noise which makes it difficult to be separated from the laser stripe. To demonstrate this, Fig. 1c, d shows the images captured with a narrow band filter and that captured without the filter respectively. The high red contrast of the laser in Fig. 1d can be observed from the image. Therefore, a software-based colour filtration is proposed to segment the laser stripe. The original image to be used is depicted in Fig. 2a. The process starts with the application of an averaging filter described by Eq. (1) in order to spread the laser red colour around neighbouring pixels. The average filtering process is necessary to smoothen high intensity saturated pixels (nearly white coloured) that may be present in the centre of the laser due to the non-uniform intensity of the laser light and also in order to suppress high intensity noises in the background. The result of applying the averaging filter is shown in Fig. 2b.

$$F(i,j) = \frac{1}{LW^2} \sum_{i}^{LW} \sum_{j}^{LW} I(i,j) \tag{1}$$

where $LW = 10$ and it is the maximum expected laser width, $I(i,j)$ is the image intensity at row i and column j and $F(i,j)$ is the filter result at row i and column j.

The processed image is then converted from an RGB colour space into *hue*, *saturation*, *value* (HSV) colour space. This is a major step in order to extract the red colour of the laser line from the image. The hue represents the colour itself. The value of the hue range is between 0 and 360 (0 to 1 if normalised); saturation indicates the degree to which the hue differs from a neutral grey, or simply, it indicates the purity of a colour. The saturation values varies from 0, which means no colour saturation (pure white), to 1 (pure colour), which is the fullest saturation of a given hue at a given illumination. The value

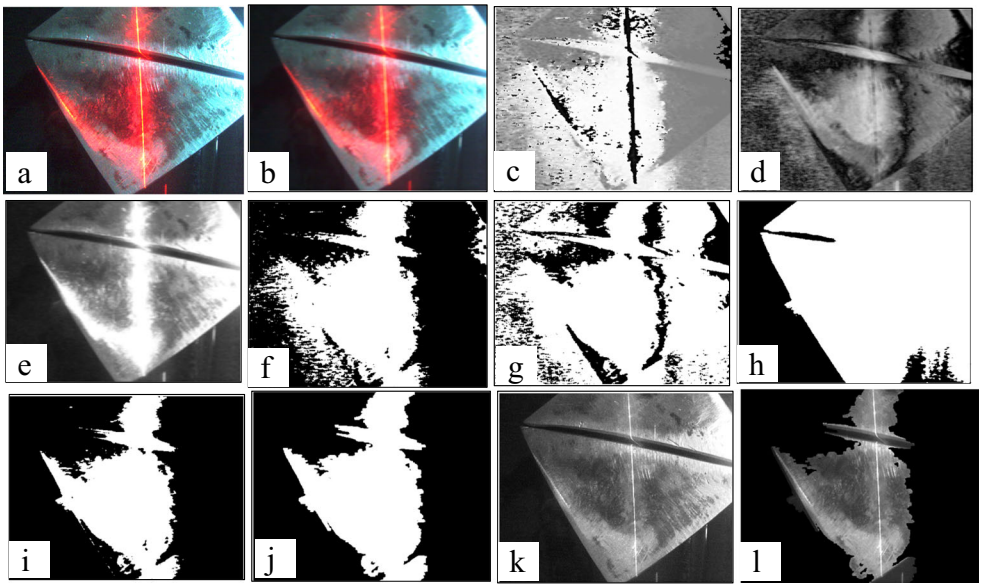

Fig. 2 **a** Original image, **b** the averaged image of Fig. 2a, **c** hue channel of the input image, **d** saturation channel of the image, **e** value channel of the input image, **f** generated hue mask (M_1), **g** generated saturation mask (M_2), **h** generated value mask (M_3), **i** the mask generated after thresholding HSV masks, **j** the processed mask after morphological operation and blob analysis, **k** the grey image of the RGB input image and **l** the masked segmented image after colour processing and median filtering

is the illumination level or measure of the level of brightness. After converting the processed image into HSV colour space, the resulting HSV channels are shown in Fig. 2. It can be observed from the hue image of Fig. 2c that the red laser line region has the least hue value, represented by black in the hue image. And, the background of the input image has higher hue values represented by the brighter colour. The saturation image of Fig. 2d also shows red laser region of which the brightest colour indicates the purity of the colour combinations of the input image. The value image of Fig. 2e depicts the illumination of the input image with the laser region showing higher illumination. The three HSV channels are thresholded by using Eqs. (2), (3) and (4). Three masks are generated shown in Fig. 2f, g, h respectively. The final exclusion mask is generated by using (5) as shown in Fig. 2i. The threshold values for hue channel are chosen to cover all the range of red region in the hue value ranges. The saturation and value thresholds are chosen to allow poor contrast laser stripe typical characteristics of a low-quality laser to be accommodated.

$$M_1 = \begin{cases} H(i,j) < 0.1 & 1 \\ H(i,j) > 0.9 & 1 \\ \text{otherwise} & 0 \end{cases} \quad (2)$$

$$M_2 = \begin{cases} S(i,j) > 0.2 & 1 \\ \text{otherwise} & 0 \end{cases} \quad (3)$$

$$M_3 = \begin{cases} V(i,j) > 0.2 & 1 \\ \text{otherwise} & 0 \end{cases} \quad (4)$$

$$M = M_1 \cap M_2 \cap M_3 \quad (5)$$

where M_1, M_2 and M_3 are the thresholded masked for the H, S and V channels respectively, i ,j is the row and column numbers and M is the final exclusion mask.

It can be observed that the exclusion mask has multiple binary objects. Hence, there is a need to remove all other binary objects in the mask except one object which includes the laser line. Two steps are followed in order to have a mask with only one object. The first step is applying morphological dilation operation on the mask to close and connect disconnected object that may belong together. The second is applying blobbing analysis on the resulting mask to remove all the binary objects, except the longest object. The final exclusion mask is shown in Fig. 2j. The three-channel RGB image need to be converted into single channel that can be masked. The conversion is either by converting to grey image or selecting the red channel depending on the laser quality. The resulting single-channel image is shown in Fig. 2k. The generated exclusion mask in Fig. 2j is then applied to the single-channel grey image. The final segmented image after the masking operation is further filtered with a conventional square median filter with a kernel of 5 by 5 in order to filter some of the white and long trail noises that may be created by the reflection of the laser light on an object or due to the welding arc light spatter. The resulting image is shown in Fig. 2l. It can be observed that some of the small high-frequency reflections of the input image are suppressed and also the salt-and-peppered particle noises are removed. This resulting image is the image that would be used in the subsequent image processing steps.

Step 2: *Laser peak detection*

The laser peak detection is aimed at extracting the profile pixels that will represent the laser stripe during the feature point extraction stages. Typical intensity distribution of the processed image for two of its rows marked in Fig. 3a as 600th and 700th which are shown in Fig. 3e. It can be observed that each row has its peek pixel somewhere within the laser stripe region. To extract the peak in each row, the maximum intensity pixel is taken in each row as the position of the

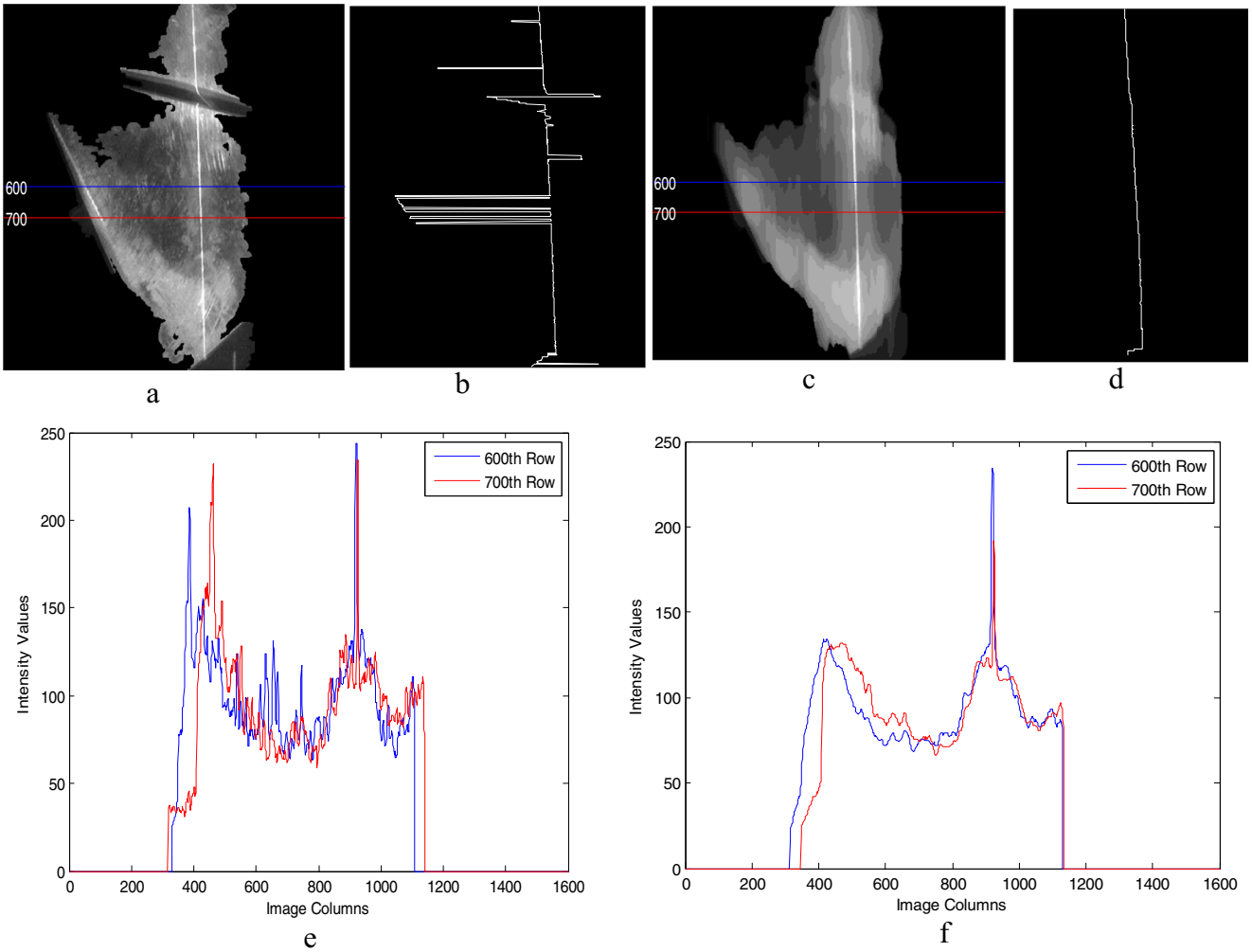

Fig. 3 **a** The processed image from Fig. 2l. **b** Typical intensity distribution of the two rows marked in **a**. **c** The peak line extracted from the image. **d** The enhanced image using vertically oriented median filter. **e** Typical intensity distribution of the enhanced image. **f** The peak line extracted from the enhanced image

laser stripe in that row. However, as shown in Fig. 3e, there can be more than one maximum pixel of the same intensity. A peak extraction algorithm is proposed to extract these peaks. The algorithm is given by algorithm 1 (*appendix*). The algorithm only considers peaks that are greater than 80 % of the maximum intensity level. If a peak is less than the given threshold, the peak position is assigned to be zero and will not be considered by the subsequent processing steps. The extracted peak line from this algorithm is shown in Fig. 3b.

Table I Details of the real-time test in the study

Image processing average running time	300 ms
Image capture rate	Four images per second
Camera resolution	1600 × 1200
Video frame rates	Five frames per second
Robot travelling speed/welding speed	0.01 m per second
Welding machine wire feed rate	40 m per second

It can be observed that the extracted peak line has a lot of unnecessary breaks along its length. This is due to noisy spikes in the rows of the processed image. Therefore, in order to alleviate this problem of the noisy spikes, a novel approach is proposed which effectively improves the peak detection. The proposed approach is based on a novel oriented median filtering to enhance an oriented object in a noisy image. This new approach will treat the horizontally oriented objects as spurious noises and then effectively suppress the noisy effect that can deteriorate the performance of the peak extraction. The conventional way of applying the median filter is to select a suitable square kernel size similar to that used in the previous section (as shown in Fig. 2l). The selection of the kernel size determines the neighbourhood around the pixels to be considered and do not consider the underlying structure present in the image. As we have an image with a vertical object structure, the kernel size of the proposed median filter is selected as vertically oriented long rectangular kernel with $LW \times 200$ neigbourhood, where LW is the expected maximum width of

the laser. The size of the kernel was determined experimentally in order to produce an enhanced laser stripe in the image. The result of applying the proposed vertically oriented median filter to the processed image is shown in Fig. 3c. As it can be seen from the results, the proposed median filter emphasises the vertical laser line object in the image and attempt to cancel any object shorter than its vertical length. The effect of the filter on the intensity distribution of the image is also shown in Fig. 3f. The filter has successfully reduced some of the noisy spikes located outside of the laser stripe region. As a result, the width of the intensity distribution is reduced and the distribution has groups of spikes that can be easily differentiated. The ultimate effect of the proposed filter is clearly shown in the extracted profile result as shown in Fig. 3d.

Step 3: *Line fitting*

The extracted peak point positions are then fitted to a straight line by using polynomial curve fitting [39] algorithm. The profile points may contain empty rows with no points due to the rejection of pixels with maximum less than the given threshold in *algorithm 1* (*appendix*). This empty rows are treated as outliers and will not be considered by the line fitting algorithm. The result after the line fitting algorithm proposed in [39] is shown in Fig. 4. The line returned by the line fitting algorithm is the detected position of the laser base line as shown in Fig. 4.

2.2.2 Seam feature point extraction

The terminologies used for the feature points in this section are explained in Fig. 5. It can observed that the *deformation* region is the region along the laser stripe that contains all the three feature points. The proposed image processing steps for extracting the feature points from the detected laser stripe includes (a) vertical ROI determination, (b) junction points

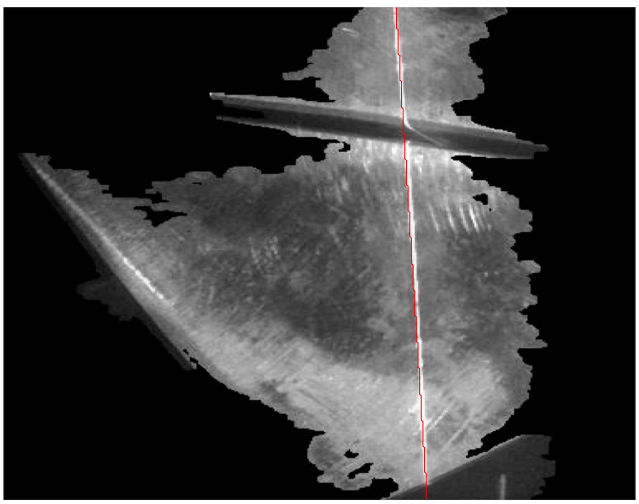

Fig. 4 Detected laser base line positions

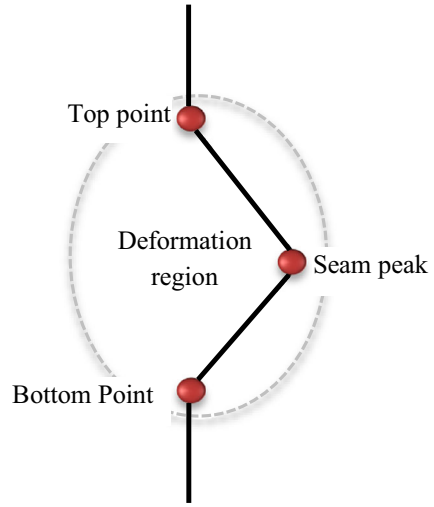

Fig. 5 The welding seam joint

labelling and grouping, (c) horizontal ROI determination and (d) determination of the feature points. The vertical ROI is extracted along the extracted laser line in order to determine the *top* and *bottom* feature points. On the other hand, the horizontal ROI is extracted in order to extract the *seam peak* feature point. It is vertically bounded by the top and bottom feature points.

Step 1: *Determination of vertical ROI*

From the original image in Fig. 2a, it is evident that the feature extraction process can only affect the region where the laser stripe is found. Marking this region as the ROI will greatly simplify the feature extraction. The vertical ROI is determined by cropping the processed filtered image (shown in Fig. 2l) around the region of the previously detected laser line. Equation (6) is used for this purpose.

$$ROI(i,c) = I(i,j) \tag{6}$$

$$\text{where } p - \frac{LW}{2} \le j \le p + \frac{LW}{2}; \qquad 0 \le i \le M;$$

where LW is the expected laser width and M is the number of rows in the image I. $I(i,j)$ is the processed image intensity at row i and column j. $ROI(i,c)$ is the ROI image. p is the column index of the previously detected laser line in the original image.

Figure 6a, b shows the ROI marked in the image and the extracted ROI image respectively. In order to clearly depict the effect of the vertical ROI, the ROI is marked on a different image containing a tilted laser object and the images are

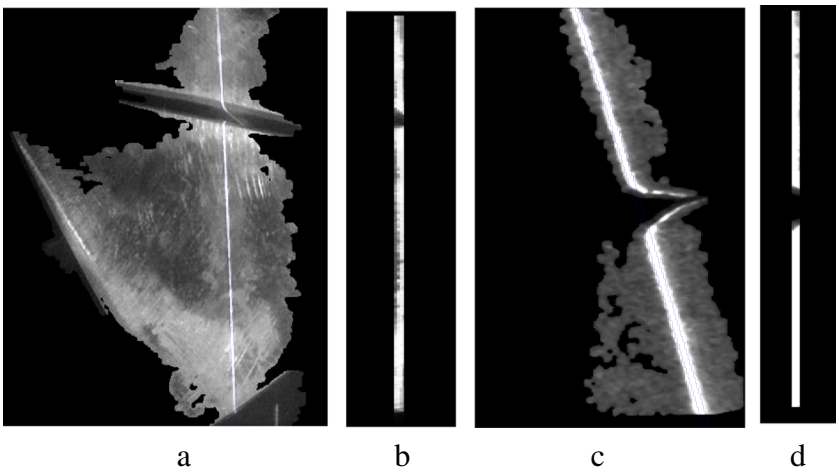

Fig. 6 **a** The ROI region marked in the original image and **b** the extracted ROI. **c** The ROI marked in another image and **d** the extracted ROI

shown in Fig. 6c, d. It can be observed that the ROI will trim some of the laser *deformation* region.

Step 2: *Labelling, grouping and selection of junction points*

Junction points are disjointed points along the laser stripe profile that correspond to the pattern produced due to the projection of the laser light on a welding joint. They are simply the points within the laser *deformation* region from which the top and buttom feature point can be extracted. However, due to inherent noise, multiple junction point groups can be found. Figure 7 shows an example of labelled junction point groups on an extracted laser stripe. Three groups of junction points are shown in the Fig. 7a. The first and third groups, which are labelled as '1' and '3' respectively, are obviously false junction groups which are due to inherent noise. On the other hand, the second group labelled as '2', is the true junction point group that corresponds to the laser *deformation* region. *Algorithm 2* (*appendix*) is used to label a laser stripe profile point as a junction point belonging to a particular group. The main idea of determining a junction point is to use the projection of the point on the fitted laser line as shown in Fig. 7b. The farther the point from the line, the more likely it will be labelled as a junction point.

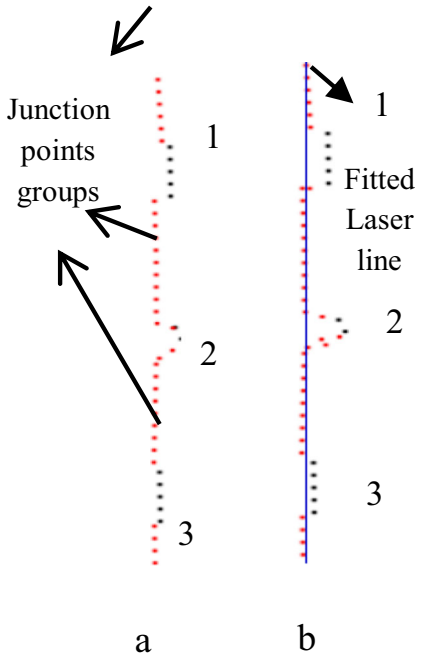

Fig. 7 **a** Labelled junction points on laser profile. **b** Fitted laser line with labelled junction points

According to the junction group selection criteria of algorithm 2, a junction group is selected by using three criteria as follows: (a) the number of points in the group, (b) the position of the group along the vertical fitted line and (c) the average maximum intensity of the group. It is evident that in moving along the laser stripe region, the deformation of the welding joint is presumed to be relatively large size of at least 5 pixels height; hence, all junction groups with number of points less than 5 pixels are discarded. Also, the deformation that corresponds to true junction group is always anchored by vertical up and down line stripe segments, hence, all junctions positioned at the beginning or at the end points in the vertical line are discarded. The remaining junction groups are evaluated based on their average maximum intensities. The average maximum intensity of a junction group is calculated by using (7).

$$\text{Average\_}Max = \frac{1}{N}\sum_{i}^{N} \max_{1\le j\le LW} F(\text{JP}(i), j) \tag{7}$$

where N is the number of points in the junction points group JP, LW is the maximum expected laser width and $F(i,j)$ is the processed image.

The group among the remaining groups with the least average maximum intensities is selected as the junction group. The result after applying algorithm 2 to the ROI image is shown in Fig. 8. In this example, there are two

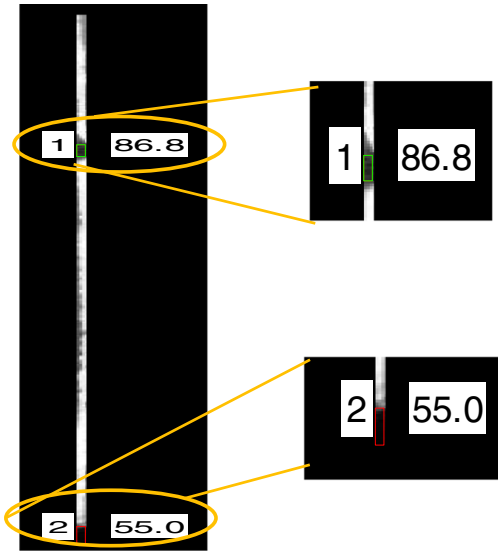

Fig. 8 Marked junction points with their respective average maximum intensities in ROI image and zoomed out from the ROI image

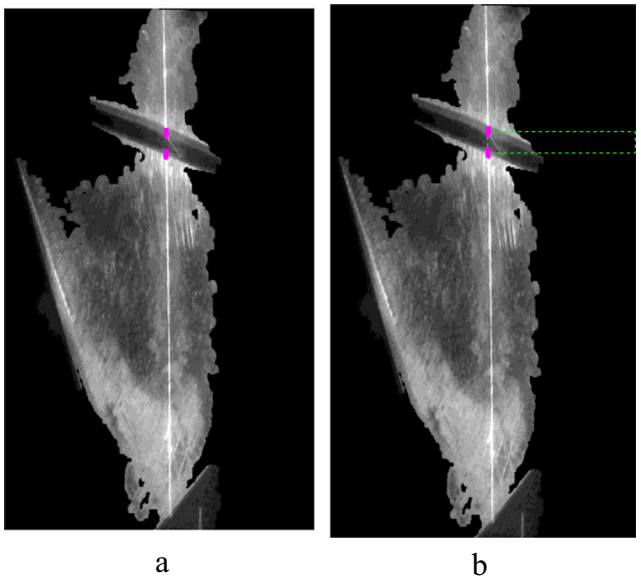

Fig. 10 Marked top and bottom point; horizontal ROI marked by the rectangle **a** before rotation correction and **c** after correction

candidate junction groups labelled as 1 and 2 respectively. The false junction group is marked in red rectangle, and the selected junction group is marked in green. It can be observed that, according to the previously stated rules, the junction group 1 from Fig. 8 is selected even though it has an average maximum intensity of 86.8 that is greater than that of group 2 with average maximum intensity of 55.0. This is because of the position of group 2 that is at the end of the stripe which violates one of the selection criteria. To further demonstrate the effect of algorithm 2, the algorithm is tested on a more complex ROI extracted from a different image as shown in Fig. 9a. Despite the number of junction groups present in the ROI, the algorithm was able to successfully apply the selection criteria and select the group 9 as the correct junction group as shown in Fig. 9b.

From the selected junction group, the first and last points in the group correspond to the top and bottom feature points. The two selected points are marked in Fig. 10a.

Step 3: *Determination of horizontal ROI*

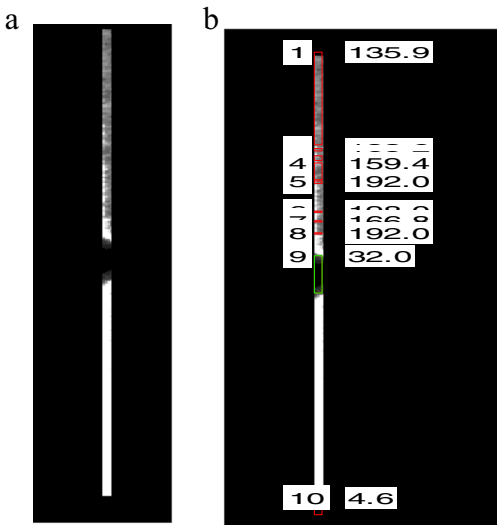

Fig. 9 Complex ROI with many junction groups. **a** Original ROI image and **b** marked junction points with their respective average maximum intensities

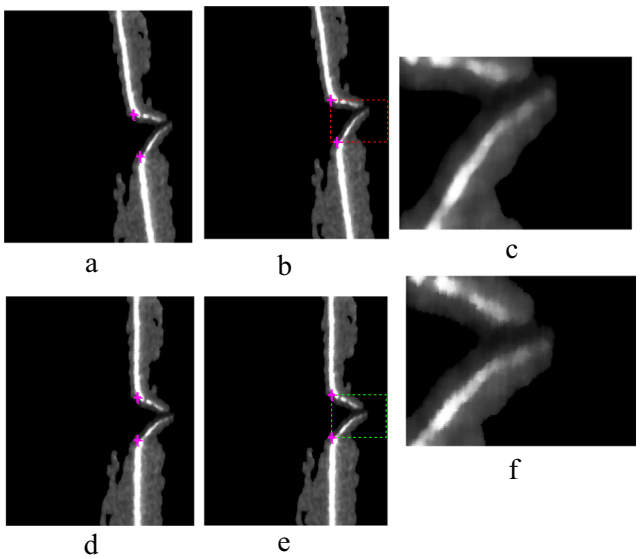

Fig. 11 Demonstration of the effect of rotation on the horizontal ROI extraction with the original image, marked ROI on the original image and extracted ROI: **a**–**c** without rotation correction and **d**–**f** with rotation correction

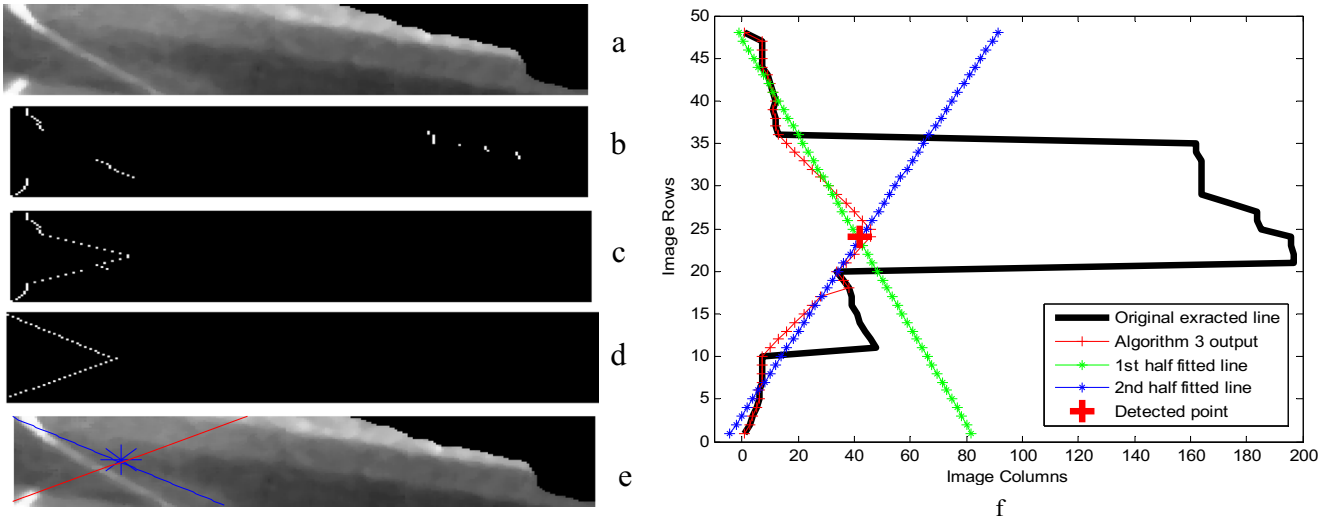

Fig. 12 Zoomed images of **a** extracted horizontal ROI, **b** extracted profile from the ROI by using algorithm 1, **c** processed profile by using algorithm 3, **d** processed profile points fitted in straight line, **e** final seam peak point detected by using algorithm 3 together with the fitted line. **f** The extracted, processed, fitted profile and detected seam peak point

The vertical region of interest marked previously only selects the region around the detected laser base line and does not account for the wider region around the *deformation* region. As such, a new ROI that will cover wider region around the stripe deformation needs to be selected in order to correctly identify the seam peak point. The new ROI can be extracted horizontally from the original processed image (shown in Fig. 2l) by using the knowledge about the position of top and bottom feature points. This is necessary in order to find the farthest point in this region that corresponds to the *seam peak* point of the welding joint. To properly select the region, the orientation of the laser stripe line must be taking into consideration. Hence, before the extraction, the tilt in the original image must be removed. The correction is performed by rotating the image with the inverse of the tilt angle θ which is calculated by using Eq. (8). The horizontal ROI is then determined by using Eq. (9).

$$\theta = -\tan^{-1}\left((Top_x - \text{Bottom}_x)\Big/\left(Top_y - \text{Bottom}_y\right)\right) \tag{8}$$

$$ROI(c,j) = I'(i,j) \tag{9}$$

$$Top'_y \le i \le \text{Bottom}'_y; \quad \text{minimum}\,(Top'_x,\ \text{Bottom}'_x) \le j \le N;$$

where θ is the tilt angle of the laser stripe with regards to vertical axis, Top_y, Top'_y, $Bottom_y$ and $Bottom'_y$ are the x and y values of the top and bottom points before and after rotating

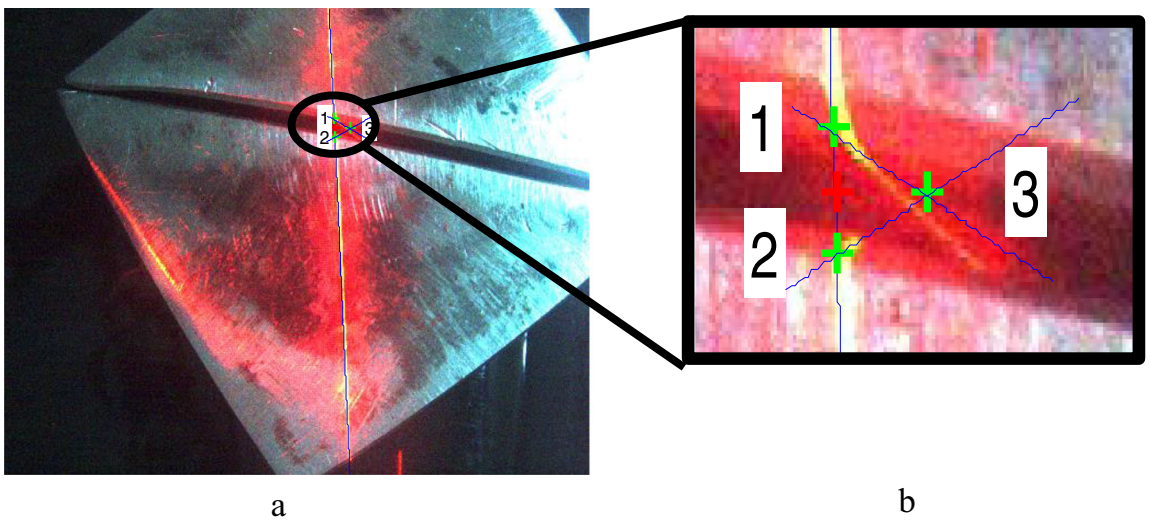

Fig. 13 Final detected points for **a** original image and **b** zoomed original image for clarity of the detected point

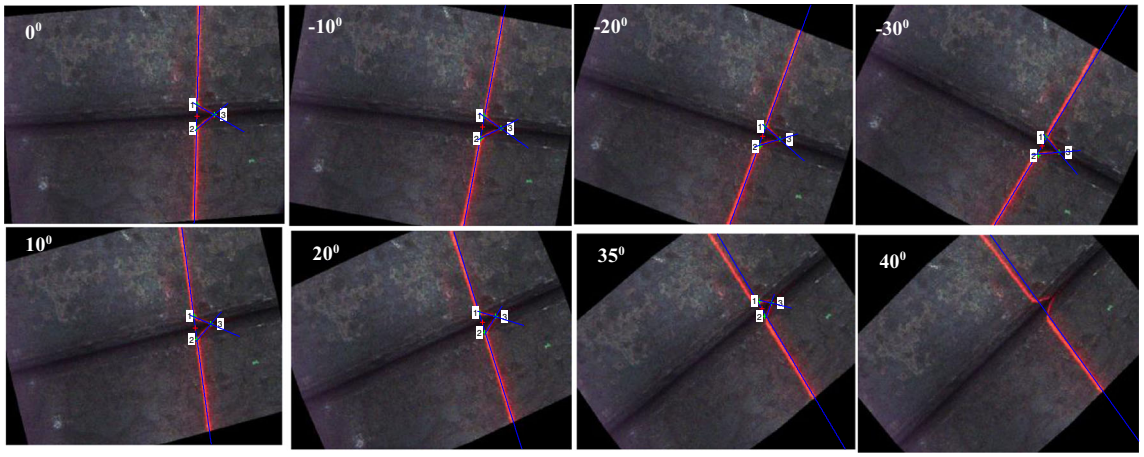

Fig. 14 Extracting the feature points from rotated laser stripe images

with θ respectively. N is the number of columns in the image I. $I'(i,j)$ is the processed image intensity at row i and column j rotated with the angle θ. $ROI(c,j)$ is the ROI image.

The marked horizontal ROI after the rotation correction is shown in Fig. 10b. In order to demonstrate the needs of correcting rotation before the horizontal ROI extraction, an image with a very wide seam and a rotated laser stripe is used as shown in Fig. 11. Due to the slight rotation, if the horizontal ROI is extracted without correcting the rotation as shown by Fig. 11a–c, some of the laser deformation region may not be selected and could lead to the deselection of the seam peak point region. However, the ROI will be properly extracted if the rotation is corrected first before the extraction step as shown in Fig. 11d–f.

Step 4: *Detection of seam peak point*

The seam peak point is the uttermost or farthest point from the laser stripe line that correspond to the end of the laser obstruction on the welding seam. The position of the point is crucial because any small background noise could deter or completely change the position of the point and subsequently change the orientation of the whole seam from the laser stripe perspective. *Algorithm 3* (appendix) is used in determining this point. First, the profile points are extracted from the horizontal ROI (shown in Fig. 12a) by using algorithm 1, and the resulting image is shown in Fig. 12b. From the extracted profile, breaks and some out of place noisy points can be observed. These points are filtered with algorithm 3. The algorithm works by dividing the laser stripe profile into two parts (upper and lower) and scan each part independently. Since the top and bottom feature points already determined are in the extracted profile with top point being the first point in the stripe and the bottom point being the last point. Hence, the first point in the upper part is the top point and last point in lower part is the bottom point. Therefore, the upper part is scanned by starting from the first point to its last point. On the other hand, the lower part is scanned from the last to its first point. During the scanning, the change in column index between a row and its previous row is checked in order to determine whether it is within the given limit. If it is out of the limit, the column index of the current row is changed to the limit value. The limit of $-LW \leq Column\ index \leq LW$ is chosen. This is based on the assumption that for consecutive rows, the laser profile point column position in these rows should be as close to each other as possible, at least within the laser

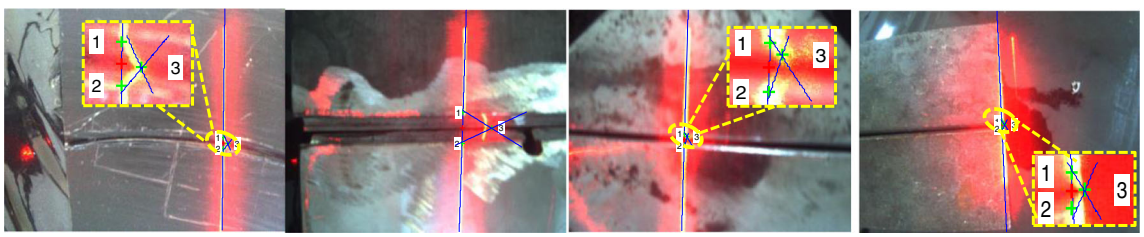

Fig. 15 High-quality laser with strong reflection image result

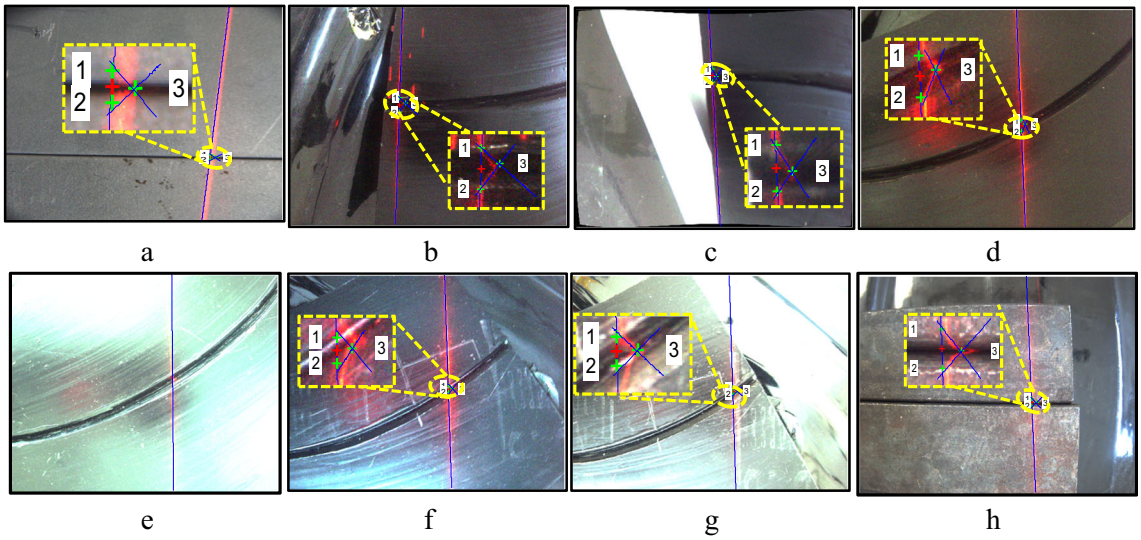

Fig. 16 Low quality and complex background laser image results

width. After the scanning, two new profiles will be generated from the two parts. The two profiles when combined makes up the processed profile shown in Fig. 12c. The two profiles are then fitted into a straight line by using the polynomial fitting algorithm. The result is shown in Fig. 12d. The intersection of the two lines is selected as the detected peak shown in Fig. 12e. It can be observed that the original extracted profile (shown in Fig. 12b) have been filtered and the outlier points corrected by drawing the points closer to the profile as shown in Fig. 12c. Figure 12f shows elaborately the relationship between the original profile, processed profile, fitted lines and the detected seam peak point when plotted on a graph.

After the laser stripe detection and the feature point extraction stages, the top, bottom and seam peak feature points have been successfully extracted as shown Fig. 13.

3 Results and evaluation

The proposed algorithm is implemented on a Windows 8 computer with Intel Core i7 2.0 GHz processor, 8 GB RAM. The computer is directly connected to the robot and the camera. The algorithm performance is evaluated in two ways: (1) image processing results' evaluation and (2) real-time robot motion results.

To evaluate the effectiveness of our proposed image processing and feature extraction method, four different set of images are used: (1) images containing rotated laser stripe, (2) high-quality laser with strong reflection

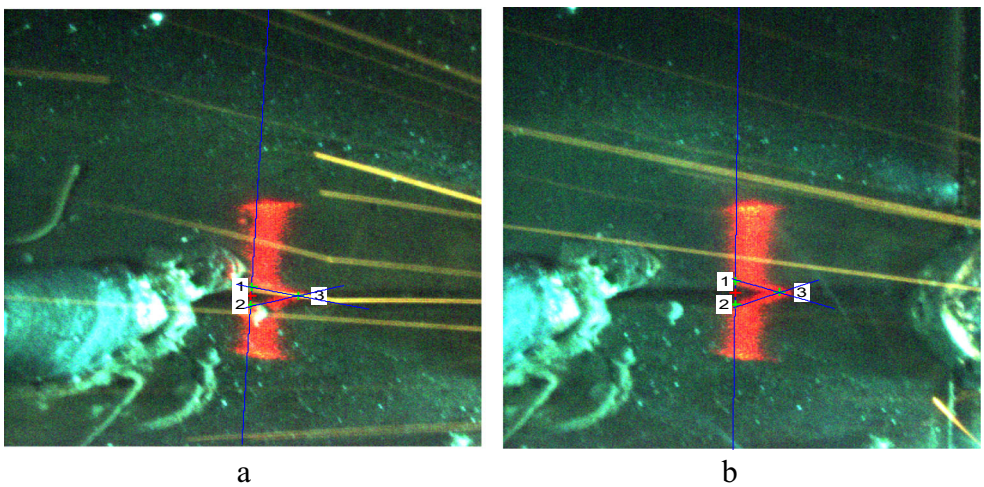

Fig. 17 Welding images without a narrow band filter result

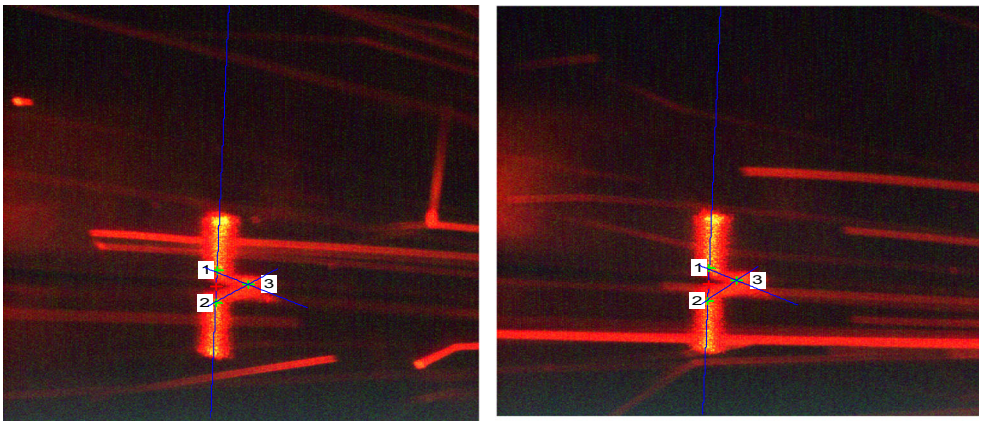

a b

Fig. 18 Welding images with a narrow band filter result

images, (3) low-quality and complex background laser images, (4) welding images with narrow band filter and (5) welding images without narrow band filter. The aim is to test the robustness of the proposed approach against rotation, poor-quality laser, background complexities, reflection and welding noise. For the rotation, the results are shown in Fig. 14. Because part of the algorithm implementation relies on vertical objects, the rotation test is important to know how much the algorithm will be affected when the laser is rotated. The images contain laser rotated from −30° to 40° with anti-clockwise been the positive direction. From the results, it can be observed that as the rotation increases the detected base line got slightly out of phase. However, due to robustness of the feature extraction stage, the position of the feature points is not affected. The algorithm fails when the rotation reaches 40°. However, the results indicate that the rotation of the laser up to a certain degree does not affect the result of the extracted seam feature points.

The results for the high-quality laser with strong reflection images are shown in Fig. 15. Due to the nature of the laser, the reflection in the image is very strong. However, the algorithm has successfully detected the seam positions in these images. The result in Fig. 15c shows the extracted seam peak points which is slightly not at the expected location. This is because, during the seam peak extraction stage, the outmost laser pixels in this region due to their slightly lower intensity will be assumed to be part of reflections and thresholded.

Figure 16 The result for the low-quality laser images. The algorithm successfully detects all the seam feature points in all the images except that of Fig. 16d. This is because the laser in this image is badly disrupted by the strong lightening source. It is important to note despite the complexity of Fig. 16**c** and the strong illumination of Fig. 16**f** images that the algorithm was able to detect the feature points in these cases. The results for welding images captured with and without the narrow band filter are shown in Figs. 17 and 18 respectively. The distinction between these two set of images can be examined. For the images captured without the filter, the red laser is well pronounced and the proposed algorithm was able to accurately extract the feature points in them despite the strong arc white noise present. For the images with the filter, the laser is somehow normalised with the welding noise and its contrast greatly affected. However, the proposed algorithm was able to extract the feature points accurately. This can be attributed to the proposed oriented median filtering that suppress the horizontally oriented randomly distributed welding noise

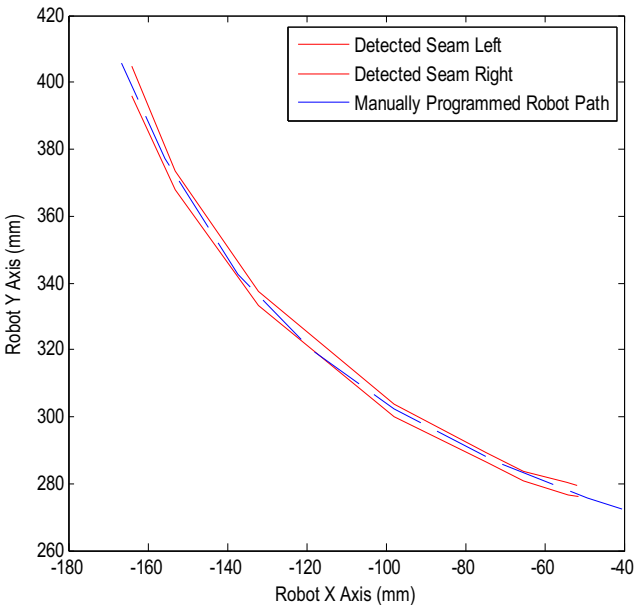

Fig. 19 Robot motion result compared with the result from the extracted seam path

In order to evaluate the effectiveness of the proposed method by using the robot motion, the algorithm was tested in real time with the robot. During the test run, the extracted image coordinates were converted to the robot world coordinates by using Eqs. (10), (11) and (12). Equation (10) was obtained after camera calibration, where the camera extrinsic and intrinsic parameters were determined.

$$s\begin{bmatrix} u \\ v \\ 1 \end{bmatrix} = \begin{bmatrix} 2006.68 & 0 & 791.77 \\ 0 & 2006.10 & 590.38 \\ 0 & 0 & 1 \end{bmatrix} \tag{10}$$

$$\begin{bmatrix} 0.09 & -1.00 & -0.04 \\ -1.00 & -0.09 & 0.01 \\ -0.01 & 0.04 & -1.00 \end{bmatrix}$$

$$\begin{bmatrix} X \\ Y \\ 2.5 \end{bmatrix} + \begin{bmatrix} -8.24 \\ 139.88 \\ 110.96 \end{bmatrix}$$

$$X_R = X_{TCP} - X \tag{11}$$

$$Y_R = Y_{TCP} - Y \tag{12}$$

where (u, v) are the extracted image coordinates, (X, Y) are the converted camera coordinates, (X_{TCP}, Y_{TCP}) are the current position of the tool centre point (TCP) and (X_R, Y_R) are the converted final robot coordinates.

The details of the real-time test relevant to this work is shown in Table I below.

From Table I, it can be observed that the average image processing running time was found to be just about 300 ms for an image with 1200 × 1600 size. This means that it can process at least three images in 1 s. For a welding process which is usually a very slow process (like the 0.01 m/s used, which depends on the welding scenario), processing of three images in a second is practically contented.

The robot was first programmed manually to approximately follow the centre path of the test curvature workpiece as shown in Fig. 19. The trajectory of the robot teach and playback is shown in Fig. 19 as a dashed line. For the same path, the robot has been guided by the proposed algorithm and the extracted seam path is labelled as the detected seam left and the detected seam right. It is obviously evident from the figure

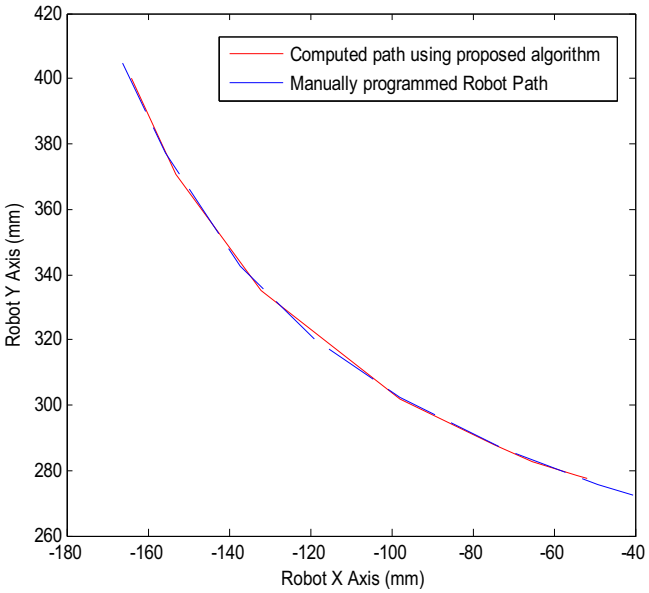

Fig. 20 Robot motion result compared with the result from the computed curve path from the extracted seam

that the proposed seam finding method is successful in extracting the seam path. From the extracted seam path, the centroid coordinates in the path can be computed as the robot path. Figure 20 shows the comparison of the computed robot path with the actual manually programmed robot path. The two paths could be observed to approximately fit each other.

4 Conclusion

In this paper, we present a novel method that can effectively find the seam geometrical information by using active vision. It utilises a combination of colour processing, median filtering and pixel neighbourhood search. It was implemented and tested in various background complexities, laser type and seam sizes. It has proven to be effective with less expensive low-quality laser images and robust to reasonably rotated laser stripes. Using the proposed approach, we have been successful in implementing an active vision system with the following advantages: (1) does not use the conventional narrow band filter for the laser wavelength selection which results to cost reduction and increased laser contrast, (2) be able to work with very low-quality laser, (3) robust to laser rotation and (4) effective in extracting the required geometrical features.

Acknowledgments The authors would like to acknowledge the support provided by The Scientific and Technological Research Council of Turkey-TÜBİTAK (grant no. 114M756) for conducting this research work.

Appendix

Algorithm 1:

```
Laser Line Peak Detection (I, Laser_Width, Threshold)
  Parameters List:
    Laser_Width: expected width of laser
    Threshold:  minimum laser intensity
    Laser_Line: array containing column index in each row  of the laser stripe line
    row: index of the current row

01  INITIALISE Laser_Line=ARRAY[number of rows of image I ]; row=1;
02  LOOP FOR EACH row in the image I
03      FIND maximum intensity in the row
04      IF  maximum intensity  IS GREATER THAN  Threshold
05          FIND all columns equal maximum intensity
06          GROUP maximum intensity columns that is at least one column apart
07            SELECT the GROUP that has the highest number of elements and with number of elements less
than Laser_Width
08          SET Laser_Line[row]=column index of centre element in the selected group
09      ELSE
10           SET Laser_Line[row]=0
11      ENDIF
12      SET row=row+1;
13  END LOOP
14  RETURN Laser_Line
```

Algorithm 2:

```
Junction Points labelling Algorithm (ROI, Threshold)
   Parameter List:
      ROI: the extracted ROI
      Threshold: cut off intensity value for non-laser line regions
      Junction_Points: binary array indicating if a row is a Junction point or not
      row: index of the current row

01  INITIALISE Junction_Points=ARRAY [number of rows of ROI ]=0;  row=1;
02  LOOP FOR EACH row in the ROI
03      FIND maximum intensity in the row
04      IF maximum intensity > Threshold
05       SET Junction_Points [row]=1
06      END IF
07     SET row=row+1;
08  END LOOP
09  GROUP Junction_Points that are at least more than one row apart
10  SELECT the GROUP that certisfy the junction group selection criteria
11  SET Junction_Points [NOT Selected GROUPs]=0
12  RETURN Junction_Points
```

Algorithm 3:

```
Seam Peak Detection Algorithm (ROI, Laser_Width)
  Parameter List:
    seam_ROI, ROI , Line_1 and Line_2: vectors containing the seam
          point column indexes of each row of the seam ROI
    Laser_Width: expected width of laser
    current_Ind: seam point column index in the current row;
    prev_Ind: seam point column index of the previous row
    row: index of the current row;
    rows: total number of rows in the ROI; half_rows: rows/2
    Zero_Count: number of rows with zero column index after the last Non-zero index row
    seam_peak: row index of the seam peak position

01:  SET seam_ROI=ROI(RANGE(1 TO half_rows));
02:  INITIALISE row=1; prev_Ind=seam_ROI[row]; Zero_Count=0;
03:  LOOP FOR EACH row in the seam_ROI
04            SET current_Ind=seam_ROI[row]
05            IF absolute(d) > Zero_Count * Laser_Width
06                  Zero_Count=Zero_Count+1;  CONTINUE LOOPING;
07            ENDIF
08            SET d=current_Ind-prev_Ind
09            IF absolute(d) > Zero_Count * Laser_Width
10                  IF d > 0;  SET current_Ind=prev_Ind+Laser_Width;
11                    ELSE   SET current_Ind=prev_Ind-Laser_Width;
12                ENDIF
13          ENDIF
14          SET Zero_Count=0;  prev_Ind=current_Ind;  seam_ROI[row]=current_Ind; row=row+1;
15       END LOOP
16:  SET Line_1=LINE FITTING(seam_ROI);
17          SET seam_ROI=ROI(RANGE(rows TO half_rows));  Goto Line 02
18          SET Line_2=LINE FITTING(INVERSE OF seam_ROI)
19          SET seam_peak=INTERSECTION OF Line_1 AND Line_2
20  RETURN seam_peak
```

References

1. Pires JN, Loureiro A, Bölmsjo G (2006) *Welding robots: technology, system issues and application*. Springer Science & Business Media
2. He-Xi L, Yong-Hua S, Guo-Rong W, Xiao-Xi Z (2009) Automatic teaching of welding robot for 3-dimensional seam based on ant colony optimization algorithm. In *Intelligent Computation Technology and Automation, 2009. ICICTA'09. Second International Conference on* (Vol. 3, pp. 398–402). IEEE
3. Ryberg A, Ericsson M, Christiansson AK, Eriksson K, Nilsson J, Larsson M (2010) Stereo vision for path correction in off-line programmed robot welding. In *Industrial Technology (ICIT), 2010 I.E. International Conference on* (pp. 1700–1705). IEEE
4. Kim P, Rhee S, Lee CH (1999) Automatic teaching of welding robot for free-formed seam using laser vision sensor. *Opt Lasers Eng* 31(3):173–182
5. Nele L, Sarno E, Keshari A (2013) Modeling of multiple characteristics of an arc weld joint. *Int J Adv Manuf Technol* 69(5–8): 1331–1341
6. Park YW, Rhee S (2008) Process modeling and parameter optimization using neural network and genetic algorithms for aluminum laser welding automation. *Int J Adv Manuf Technol* 37(9–10):1014–1021
7. Chaki S, Shanmugarajan B, Ghosal S, Padmanabham G (2015) Application of integrated soft computing techniques for optimisation of hybrid CO 2 laser–MIG welding process. *Appl Soft Comput* 30:365–374
8. Cook GE, Andersen K, Fernandez KR, Shepard ME, Wells AM Jr (1987). Electric arc sensing for robot positioning control. *IFS(Publications) Ltd., Robotic Welding,* 181–216
9. Fridenfalk M (2003) *Development of intelligent robot systems based on sensor control*. Lund University
10. Fang Z, Xu D, Tan M (2013) Vision-based initial weld point positioning using the geometric relationship between two seams. *Int J Adv Manuf Technol* 66(9–12):1535–1543

11. Dinham M, Fang G (2013) Autonomous weld seam identification and localisation using eye-in-hand stereo vision for robotic arc welding. *Robot Comput Integr Manuf* 29(5):288–301
12. Shen HY, Wu J, Lin T, Chen SB (2008) Arc welding robot system with seam tracking and weld pool control based on passive vision. *Int J Adv Manuf Technol* 39(7–8):669–678
13. Gao X, Ding D, Bai T, Katayama S (2011) Weld-pool image centroid algorithm for seam-tracking vision model in arc-welding process. *IET Image Process* 5(5):410–419
14. Chen SB, Chen XZ, Qiu T, Li JQ (2005) Acquisition of weld seam dimensional position information for arc welding robot based on vision computing. J Intell Robot Syst 43(1):77–97
15. Chen, X. Z., Huang, Y. M., & Chen, S. B. (2012). Model analysis and experimental technique on computing accuracy of seam spatial position information based on stereo vision for welding robot. *Industrial Robot: An International Journal*, 39(4), 349–356
16. Chen X, Chen S, Lin T, Lei Y (2006) Practical method to locate the initial weld position using visual technology. *Int J Adv Manuf Technol* 30(7–8):663–668
17. Chen, X. Z., & Chen, S. B. (2010). The autonomous detection and guiding of start welding position for arc welding robot. Industrial Robot: *An International Journal*, 37(1), 70–78
18. Muhammad, J., Altun, H., & Abo-Serie, E. (2016). Welding seam profiling techniques based on active vision sensing for intelligent robotic welding. *Int J Adv Manuf Technol*, 1–19
19. Hang, K., & Pritschow, G. (1999). Reducing distortions caused by the welding arc in a laser stripe sensor system for automated seam tracking. In Industrial Electronics, 1999. ISIE'99. *Proceedings of the IEEE International Symposium on* (Vol. 2, pp. 919–924). IEEE
20. Huang W, Kovacevic R (2012) Development of a real-time laser-based machine vision system to monitor and control welding processes. *Int J Adv Manuf Technol* 63(1–4):235–248
21. Li Y, Li YF, Wang QL, Xu D, Tan M (2010) Measurement and defect detection of the weld bead based on online vision inspection. Instrum Meas, IEEE Transactions on 59(7):1841–1849
22. Sung K, Lee H, Choi YS, Rhee S (2009) Development of a multi-line laser vision sensor for joint tracking in welding. *Weld J*
23. Huang, W., & Kovacevic, R. (2011). A laser-based vision system for weld quality inspection. *Sensors*, 11(1), 506–521
24. Li, Y., Wang, Q. L., Li, Y. F., Xu, D., & Tan, M. (2008, May). On-line visual measurement and inspection of weld bead using structured light. In *Instrumentation and Measurement Technology Conference Proceedings, 2008. IMTC 2008. IEEE* (pp. 2038–2043). IEEE
25. Naidu DK, Fisher RB (1991) A comparative analysis of algorithms for determining the peak position of a stripe to sub-pixel accuracy. In *BMVC91* (pp. 217–225). Springer London
26. Usamentiaga R, Molleda J, García DF (2012) Fast and robust laser stripe extraction for 3D reconstruction in industrial environments. *Mach Vis Appl* 23(1):179–196
27. Haug K, Pritschow G (1998) Robust laser-stripe sensor for automated weld-seam-tracking in the shipbuilding industry. In *Industrial Electronics Society, 1998. IECON'98. Proceedings of the 24th Annual Conference of the IEEE* (Vol. 2, pp. 1236–1241). IEEE
28. Gong, Y., Dai, X., & Li, X. (2010, April). Structured-light based joint recognition using bottom-up and top-down combined visual processing. In *Image Analysis and Signal Processing (IASP), 2010 International Conference on* (pp. 507–512). IEEE
29. Shi, Y. H., Wang, G. R., & Li, G. J. (2007, May). Adaptive robotic welding system using laser vision sensing for underwater engineering. In *Control and Automation, 2007. ICCA 2007. IEEE International Conference on* (pp. 1213–1218). IEEE
30. Kim, J. W., & Bae, H. S. (2005). A study on a vision sensor system for tracking the I-butt weld joints. *J Mech Sci Technol*, 19(10), 1856–1863
31. Xu, D., Tan, M., Zhao, X., & Tu, Z. (2004). Seam tracking and visual control for robotic arc welding based on structured light stereovision. International Journal of Automation and Computing, 1(1), 63–75
32. Xu, D., Wang, L., & Tan, M. (2004). Image processing and visual control method for arc welding robot. In Robotics and Biomimetics, 2004. ROBIO 2004. IEEE International Conference on (pp. 727–732). IEEE
33. Xu, D., Jiang, Z., Wang, L., & Tan, M. (2004, December). Features extraction for structured light image of welding seam with arc and splash disturbance. In *Control, Automation, Robotics and Vision Conference, 2004. ICARCV 2004 8th*(Vol. 3, pp. 1559–1563). IEEE
34. Kim, J. S., Son, Y. T., Cho, H. S., & Koh, K. I. (1996). A robust visual seam tracking system for robotic arc welding. Mechatronics, 6(2), 141–163
35. Kim, J. S., Son, Y. T., Cho, H. S., & Koh, K. I. (1995, August). A robust method for vision-based seam tracking in robotic arc welding. In *Intelligent Control, 1995., Proceedings of the 1995 IEEE International Symposium on* (pp. 363–368). IEEE
36. Sicard, P., & Levine, M. D. (1989). Joint recognition and tracking for robotic arc welding. Systems, Man and Cybernetics, IEEE Transactions on, 19(4), 714–728
37. Nan, H., Beattie, R. J., & Davey, P. G. (1988). A rule-based system for interpreting weld seam images. The International Journal of Advanced Manufacturing Technology, 3(3), 111–121
38. Xiao, Y., Zou, J. J., & Yan, H. (2001). An adaptive split-and-merge method for binary image contour data compression. *Pattern Recogn Lett*, 22(3), 299–307
39. Pavlidis, T., & Horowitz, S. L. (1974). Segmentation of plane curves. IEEE transactions on Computers, (8), 860–870
40. Gu, W. P., Xiong, Z. Y., & Wan, W. (2013). Autonomous seam acquisition and tracking system for multi-pass welding based on vision sensor. *Int J of Adv Manuf Technol*, 69(1–4), 451–460
41. Ballard, D. H. (1981). Generalizing the Hough transform to detect arbitrary shapes. *Pattern Recognit*, 13(2), 111–122
42. Berkan, R. C., & Trubatch, S. (1997). Fuzzy System Design Principles. Wiley-IEEE Press